

Quantum Tunnelling Without a Barrier: Topological Classification of Coalescing Saddle Points and Their Self-Intersecting Structures

Yann Raphael Janssen

April 22, 2025

Contents

1	Introduction	3
1.1	Attosecond Physics, Laser Pulses, and the Three Step Model	3
1.2	The Transition Amplitudes, the Action S , and Saddle Points Solutions	4
1.3	Driving Laser's Electric Field	7
1.3.1	Monochromatic vs Bichromatic Fields	8
1.3.2	Collinear vs. Co-Orthogonal Fields	9
2	Quantum Tunnelling Without a Barrier	10
2.1	1D Electric Field: Saddle Point Solutions	10
2.2	Visualising Quantum Tunnelling Trajectories	11
2.3	Decreasing Mixing Angles - Coalescence	14
3	Saddle Points in a Collinear Electric Field	16
3.1	3D View Saddle Points [p_y , Real time, Imaginary Time]: Channel Structures at Coalescence	18
4	2D Extension: Co-Orthogonal Field	20
4.1	Bifurcation Theory	21
4.2	Identifying and Tracking Fold and Cusp Points	22
4.3	Nine-Fold Classification through Fold Bifurcation	23
4.4	Six-Fold Classification through Cusp Bifurcation	25
5	Conclusion	28

Abstract

Quantum tunnelling is a well-established process, and yet, a continually evolving area of research. This report presents numerical studies of quantum tunnelling induced by strong laser fields that distort the Coulomb potential barrier, enabling ionisation. This is a fundamental process in attosecond science, which seeks to observe electron dynamics in real time. Surprisingly, we identified an ionisation event occurring when the electric field is zero, meaning there is no barrier present challenging the conventional understanding of quantum tunnelling. However, detecting this is difficult, as this ionisation event's yield is extremely low. To gain a deeper understanding of the mechanisms underlying this rare process, we employ a topological saddle point analysis and bifurcation theory. Although this approach does not directly enhance the yield of this specific ionisation event (where tunnelling occurs without a barrier) but it may reveal structural features that help identify where to look for new or more detectable signatures. This is done by extending the electric field to two dimensions and examining co-orthogonal field configurations, where we uncover a complex, self-intersecting saddle point structure. This structure evolves as the mixing angle of the electric field transitions from bichromatic to a monochromatic configuration ($\theta = 90^\circ$ to $\theta = 0^\circ$), also referred to as the colour switcheroo, giving rise to fold and cusp bifurcations. These bifurcations complicate the classification of quantum trajectories due to the intertwined nature of the resulting saddle points. Using bifurcation theory, we propose a methodology for classifying these intricate structures, and offer new insights into quantum tunnelling without a barrier.

1 Introduction

1.1 Attosecond Physics, Laser Pulses, and the Three Step Model

Attosecond Physics, a groundbreaking field awarded the Nobel Prize in 2023, is the study of ultrafast light pulses that can be used to capture very short timescales to study the electron's dynamics inside the atom [1]. When the strong-field induced laser interacts with the atoms, they distort the Coulomb potential barrier. This is the force that normally keeps electrons bound to their nucleus, much like how gravity governs the moon's orbit, though on a much stronger scale [14]. These strong laser fields distort the electric field creating a barrier, allowing the electrons to quantum tunnel, a process where particles pass through barriers that classical physics says they should not be able to overcome [15].

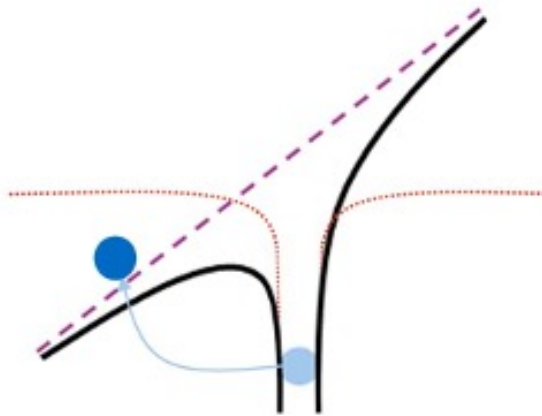


Figure 1: Example of Quantum Tunnelling

The ability of intense laser fields to ionise atoms is at the heart of attosecond physics. This interaction triggers the release of the electrons allowing observers to monitor ultrafast dynamics at the quantum level [13]. It is possible to track the electron and nuclear motion in real time. This is due to the generation of attosecond (10^{-18} sec) light pulses which is generated by driving electrons out of the atoms [13].

Above-threshold ionization (ATI) and high-harmonic generation (HHG) are the two crucial process that occur in strong field physics. ATI happens when an atom absorbs more photons than it needs to ionise, so the freed electrons end up with extra energy, which typically emits high energy photoelectrons [11].

HHG can be explained by the three-step model. Tunnel-ionisation is the first step, where the atom is ionized by a strong laser field, releasing an electron [3][8]. Propagation is the second step, where this free electron is accelerated by the laser's oscillating field, initially pushed away, but then pulled back as the field changes direction. Recombination is the third and final step, where the electron returns to the ion and recombines with it, releasing a high-energy photon in the process defining the mechanism which produces attosecond light bursts [3].

This report is focused on exploring the Tunnel-ionisation process of the three step model as it is especially crucial to understand how to control or shape these ultrafast pulses with precision.

1.2 The Transition Amplitudes, the Action S , and Saddle Points Solutions

This report will focus on numerically calculating, analysing, and later on classifying saddle point solutions to the action that describes the quantum tunnelling process for the electron inside an atom. Mathematically speaking, the saddle point is when there is a critical point laying on a surface, whose derivative is zero, but not a local minima or maxima [16]. In addition, the action is a fundamental quantity that describes the overall motion of a physical system. The semiclassical

action presented here describes electron quantum tunneling in the context of strong-field physics, specifically capturing the ionization and propagation phases as outlined in the three-step model [11],

$$S(p, t) = \int_{-\infty}^t \left[\mathcal{I}_p + \frac{1}{2} (p + A(t'))^2 \right] dt'. \quad (1)$$

where \mathcal{I}_p is the ionisation potential, p is the momentum drift, and $A(t)$ is the electrodynamic vector potential [15]. Note that this equation is arrived at by substituting the p of the kinetic energy term, $\frac{\vec{p}^2}{2}$, by $\vec{p} + e\vec{A}$ such as to incorporate the effect of the electromagnetic field on the momentum of the electron, in natural units [5].

The definition of the saddle point solutions to the action is [15],

$$\frac{\partial S}{\partial t}(p, t_s) = 0, \quad (2)$$

where these saddle points are usually complex in nature, topologically conserved, and relate to the specific ionisation times within one periodic cycle of the laser [15].

This section loosely sketches how the action S , enters the expression for the ionization amplitude, without going into too much detail, and why direct study of the action S is important. Mathematical frameworks and theoretical tools used to derive equations (1) and (2) are the keldysh theory of strong field ionisation [11], the strong force approximation (SFA) [2], and the saddle point approximation method [14].

Popruzhenko's article [11] on Keldysh, Strong Field Approximation (SFA) and other related models is largely followed in this section. Use is made of a non-perturbative approach to describe ionisation under the influence of large electromagnetic (EM) fields e.g. intense laser radiation.

In the Keldysh model the transition amplitude is given by

$$M_k(p) = -\frac{i}{\hbar} \int_{-\infty}^{+\infty} \langle \Psi_p | \hat{V}_{\text{int}}(t) | \Psi_0 \rangle dt \quad (3)$$

Where subscript K stands for Keldysh model, with the bound state wavefunction is

$$\Psi_0(\vec{r}, t) = \psi_0(\vec{r}) e^{-\frac{i}{\hbar} I_p t} \quad (4)$$

where I_p is the ionisation potential, which is the minimum energy needed to remove an electron from an atom. The interaction potential of the electron with the field is $V_{\text{int}}(\vec{r}, t) = e\vec{E}(t) \cdot \vec{r}$, the continuum state, Ψ_p , of an electron with momentum \vec{p} can be shown to be [11].

$$\Psi_p(\mathbf{r}, t) = \left(\frac{1}{2\pi\hbar} \right)^{3/2} \exp \left[\frac{i}{\hbar} \left(m\vec{v}_p(t) \cdot \vec{r} - \frac{m}{2} \int_{-\infty}^t \vec{v}_p^2(t') dt' \right) \right] \quad (5)$$

Where the velocity is $\vec{v}_p(t) = [\vec{p} + e\vec{A}(t)]/m$ and the electric field is $\vec{E}(t) = -\dot{\vec{A}}$, where $\vec{A}(t)$ is the vector potential of the EM field (the so called length gauge has been chosen) [11].

To see how the Keldysh theory relates to the Strong Field Approximation (SFA) it is useful to revisit the time dependent schrodinger equation for an electron bound by a potential $U(\vec{r})$ in a time dependent field $\vec{E}(\vec{r}, t)$ [11]:

$$i\frac{\partial}{\partial t}\Psi(\vec{r}, t) = \left[-\frac{1}{2}\Delta + U(r) + \vec{r} \cdot \vec{E}(\vec{r}, t)\right]\Psi(\vec{r}, t) \quad (6)$$

Solving the wavefunction using retarded Green's functions, it can be shown that the amplitude can be written as [11],

$$M(\vec{p}) = -\frac{i}{(2\pi)^{3/2}} \int_{-\infty}^{\infty} dt_1 e^{-iS_0(\vec{p}, t_1)} \int d^3 r_1 e^{-i\vec{v}_p(t_1) \cdot \vec{r}_1} U(r_1) \psi_0(\vec{r}_1) \quad (7)$$

with the action $S(\vec{p}, t)$ representing a phase [11],

$$S_0(\vec{p}, t) = \int_t^{\infty} \left[\frac{1}{2} \vec{v}_p(t')^2 + I_p \right] dt' \quad (8)$$

Using the above Schrodinger equation (6) we can substitute $U(r_1)\psi_0(\vec{r}_1)$ and one obtains [11]:

$$M(\vec{p}) = -\frac{i}{(2\pi)^{3/2}} \int_{-\infty}^{\infty} dt_1 \int d^3 r_1 e^{-i\vec{v}_p(t_1) \cdot \vec{r}_1 - iS_0(\vec{p}, t_1)} \vec{E}(t_1) \cdot \vec{r}_1 \psi_0(\vec{r}_1) \quad (9)$$

This expression is the Keldysh amplitude in the length gauge [11]. After spatial integration this can be written as

$$M_k(\vec{p}) = \int_{-\infty}^{\infty} dt P(\vec{p}, t) e^{-iS_0(\vec{p}, t)} \quad (10)$$

Where the phase S_0 is given by (8) and P is gauge dependent prefactor,

$$P(\vec{p}, t) = -\frac{i}{(2\pi)^{3/2}} \int d^3 r e^{-i\vec{v}_p(t) \cdot \vec{r}} V_{int}(t) \psi_0(\vec{r}) \quad (11)$$

with $V_{int}(\vec{r}, t) = e\vec{E}(t) \cdot \vec{r}$ [11]. If S_0 is large, and the phase, e^{-iS_0} , oscillates fast in time, the saddle point approximation method can be applied. Note that the action S_0 is nicely isolated in the expression for the transition amplitude (10) and direct study of the action $S_0(\vec{p}, t)$ and its saddle points $\frac{\partial S_0(\vec{p}, t)}{\partial t} = 0$ are expected to give valuable insights into the behaviour of the transition amplitude [11].

Ultimately, applying the saddle point approximation method in the SFA framework results in a summation over the discrete ionisation events [15] [11], and the amplitude takes the form,

$$M_k(\vec{p}) \approx \sum_{\alpha} \sqrt{\frac{2\pi}{iS_0''(t_{s\alpha})}} P(\vec{p}, t_{s\alpha}) e^{-iS_0(\vec{p}, t_{s\alpha})} \quad (12)$$

where $t_{s\alpha}$ is a complex solution of the saddle point equation $\frac{\partial S_0(\vec{p}, t)}{\partial t} = 0$.

It is evident that the transition amplitude is basically a summation of contributions centred around the saddle point solutions of the action. [11][12].

Saddle point solutions represent the dominant contributions to the path integral, which is an approach to calculating and summing all of the possible quantum amplitudes' paths a particle can take, and each amplitude is weighted by a phase factor involving the action [11][12]. In this formulation, the path integral approach provides a semiclassical interpretation, where the most significant paths are those where the action is stationary [11][12]. In the context of this paper, the saddle point solutions to the action (1) yield the complex ionization times (2), which indicates when the electron is most likely to tunnel out of the atom under the influence of a strong laser field [11][12][15].

1.3 Driving Laser's Electric Field

This investigation will use a two-colour laser field, comprising of two distinct frequencies, as a means to more precisely manipulating strong-field interactions. By tuning the relative phase and amplitude of the two colours, we can smoothly transition between different regimes of interaction, allowing controlled exploration of the ionisation dynamics [7]. This colour switchover refers to the continuous tuning between field configurations, not a change that occurs during a single ionisation event [7]. The colour switchover is the gradual change in dominance between the first and second harmonic, where the mixing angle θ , is responsible for this moderate replacement of the beam with its second harmonic [7]. The laser's Electric field is described as,

$$E(t) = E_1 \cos(\omega t) + E_2 \cos(2\omega t), \quad (13)$$

where $E_1 = E_0 \cos \theta$ and $E_2 = E_0 \sin \theta$ and the range for the mixing angle θ is defined to be $0^\circ \leq \theta \leq 90^\circ$ [15]. Where θ will be responsible for the transition between a bichromatic Field ($\theta = 90^\circ$) to a monochromatic field ($\theta = 0^\circ$).

1.3.1 Monochromatic vs Bichromatic Fields

For the Monochromatic case, when θ is 0° , the electric field will take this form, $E(t) = E_0 \cos(\omega t)$ [7],

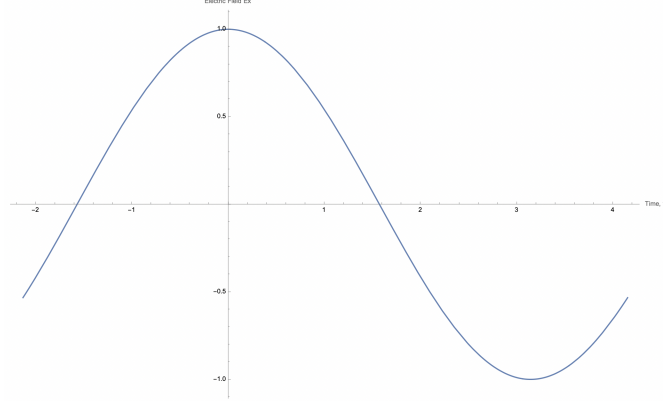


Figure 2: Monochromatic Case: Electric Field Against Time for Mixing Angles $\theta = 0^\circ$.

The laser has a pure sinusoidal shape, oscillating smoothly and symmetrically over time, it consists of a single frequency, usually referred to as the first harmonic, and it has one maxima and one minima over one periodic cycle [7].

For the Bichromatic case, when θ is 90° , the electric field will take this form, $E(t) = E_0 \cos(2\omega t)$ [7]

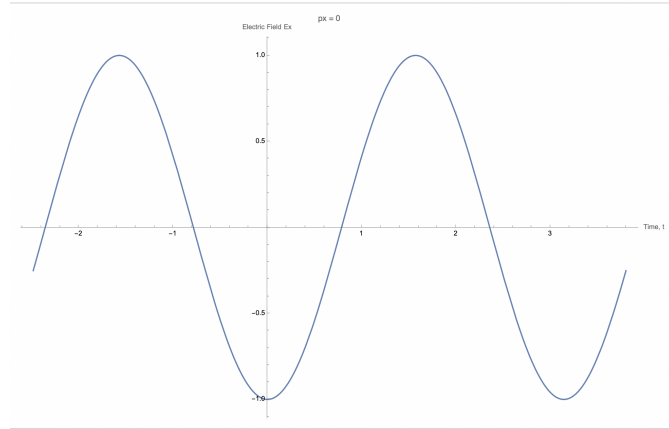


Figure 3: Bichromatic Case: Electric Field Against Time for Mixing Angles $\theta = 90^\circ$.

The laser is now asymmetrical, as it has been distorted by the superposition of two frequencies, usually referred to as the second harmonic, now generating two maxima and two minima over one periodic cycle [7].

The structure of the electric field directly influences electron dynamics, so this difference in waveform shape is key in strong-field physics [13].

1.3.2 Collinear vs. Co-Orthogonal Fields

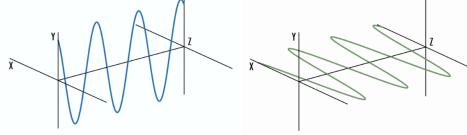


Figure 4: Two Components of the Electric Field [10].

The different orientations of the electric fields, also known as their polarisation, are shown in Figure [4], and in a two-colour field they play a crucial role in how they interact with the atom [7]. The two common configurations are collinear and co-orthogonal, where collinear has both laser fields polarised in the same axis, meaning their electric field vectors oscillate in the same direction. The resulting field is one-dimensional, the combination of their amplitudes will vary the strength of the laser but not in direction [7].

Contrastingly, co-orthogonal fields have perpendicular polarisations to one another, where the first harmonic is in one axis and the second harmonic in the other [7]. The combination of these two orthogonal orientations [Figure 4] will create a two-dimensional electric field, which is shown below in Figure [5].

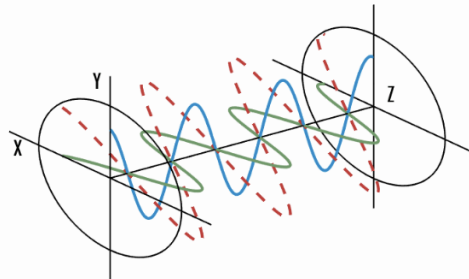


Figure 5: Example of Co-orthogonal Electric Field, Blue and Green are different orientations from Figure [4], and Red is the combination of the components [10].

2 Quantum Tunnelling Without a Barrier

2.1 1D Electric Field: Saddle Point Solutions

This analysis builds on work described in Weber's paper on Quantum Tunnelling Without a Barrier [15], where the electric field is set in one direction, such as the x-axis. The saddle point solutions for the action are given by this equation (2), where each electric field configuration generates its own saddle point solutions. The saddle point solutions are dependent on the electron's drift momentum (2). Therefore, these will vary the saddle point solutions, and this is described through a rainbow colour scheme where red is strong positive valued momenta, and violet is strong negative. The saddle points were numerically calculated and plotted along with its corresponding electric field below.

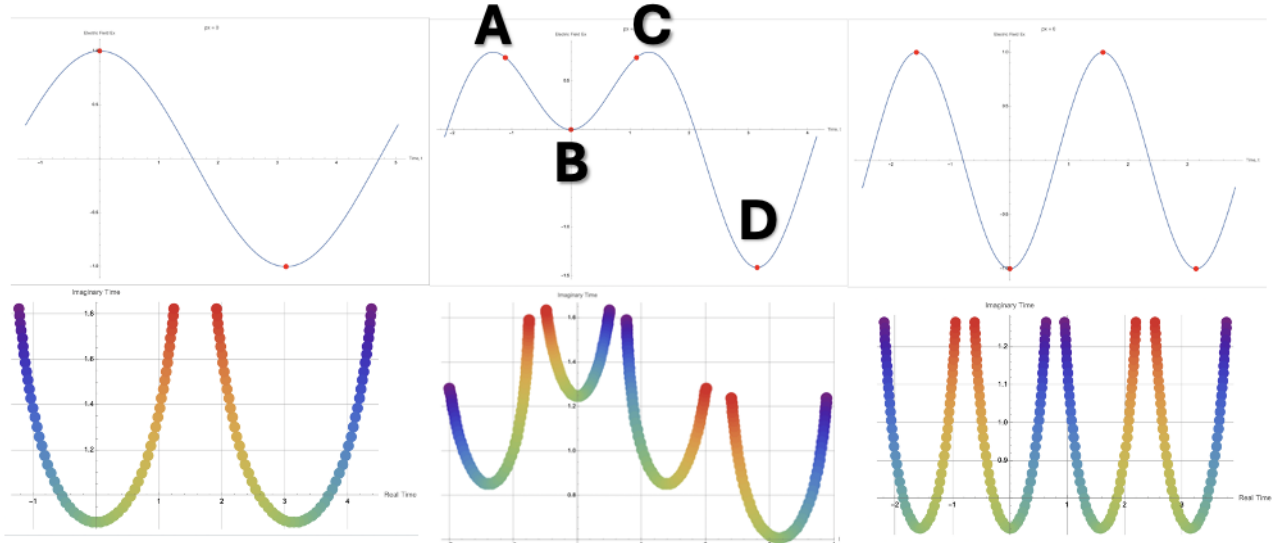


Figure 6: Top graphs: Electric Field vs Time. Bottom Graph: Saddles points in the complex plane (Horizontal Axis: Real Time and Vertical axis: Imaginary Time). Each colored dot is a saddle point solution for the corresponding electric field. Throughout this paper a rainbow colour scheme is used to denote the dependence of the electron's drift momentum on these saddle point solutions. Where red is strong positive valued momenta, and violet is strong negative. ¹

It is clear on how to distinguish the saddle points A,B,C and D for these cases. The momentum is plotted as colour in a rainbow scheme, where strong positive momenta means red, and strong negative momenta means violet. It is evident that there is a correlation between number of maxima's and minima's with the number of saddle point solutions, as shown in the top half of Figure [6], with red dots located at the peaks. The momentum drifts the solutions down to the left or right of the electric field depending on its sign (positive or negative), as shown in the bottom half of Figure [6].

¹Apologies for the small fonts in the charts for the axis, it takes a huge amount of computing time to regenerate this charts. Unfortunately, this is an ongoing theme throughout the paper, but the axis are described within the caption.

The bottom half of Figure [6] gives the ionisation times, whilst the top half shows the corresponding electric field, and where these saddle points occur. What's fascinating about this Figure is that halfway throughout the colour switchover ($\theta = 45^\circ$), there is a saddle point (red dot) when the electric field is 0 at point B. This is rather confusing, since there is no laser distorting the coloumb potential barrier at that instant. It is difficult to understand how it is possible for a particle to quantum tunnel when there is no barrier to tunnel through [15]. However the saddle point solutions to the action state that there is an ionisation event at point B, challenging the established intuition and revealing new insights (quantum tunnelling without a barrier!) [15].

2.2 Visualising Quantum Tunnelling Trajectories

To better understand the issue, the electron's tunnelling trajectories are analyzed. This will provide valuable insight about how matter behaves at the smallest scales [15]. The electron's displacement in the electric field is given by,

$$x(t) = \int_{t_s}^t (\mathbf{p} + \mathbf{A}(t')) dt' \quad (14)$$

This integration is evaluated along a two-legged contour in the complex time plane, starting from the complex-valued saddle point t_i , descending vertically to the real axis at t_i' , and then, from there the integration proceeds along the real axis, as shown in the figure below [14].

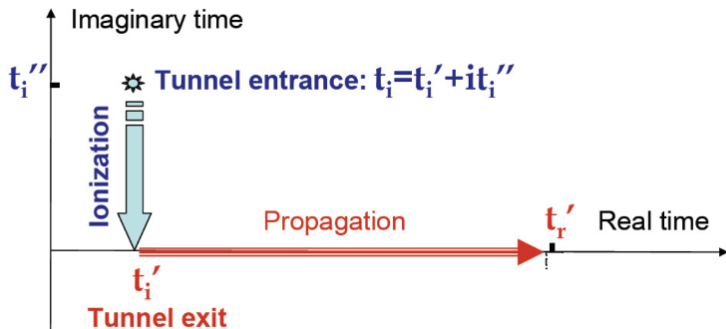


Figure 7: Contour of the Time integration in the Action Equation (1)

Due to the choice of the integral contour, it has been made a convention that imaginary time is used to represents the time taken for an electron to tunnel. Using the saddle point solutions (2), to calculate the electron's trajectories (14) the following was found for the halfway mark in the colour switchover ($\theta = 45^\circ$).

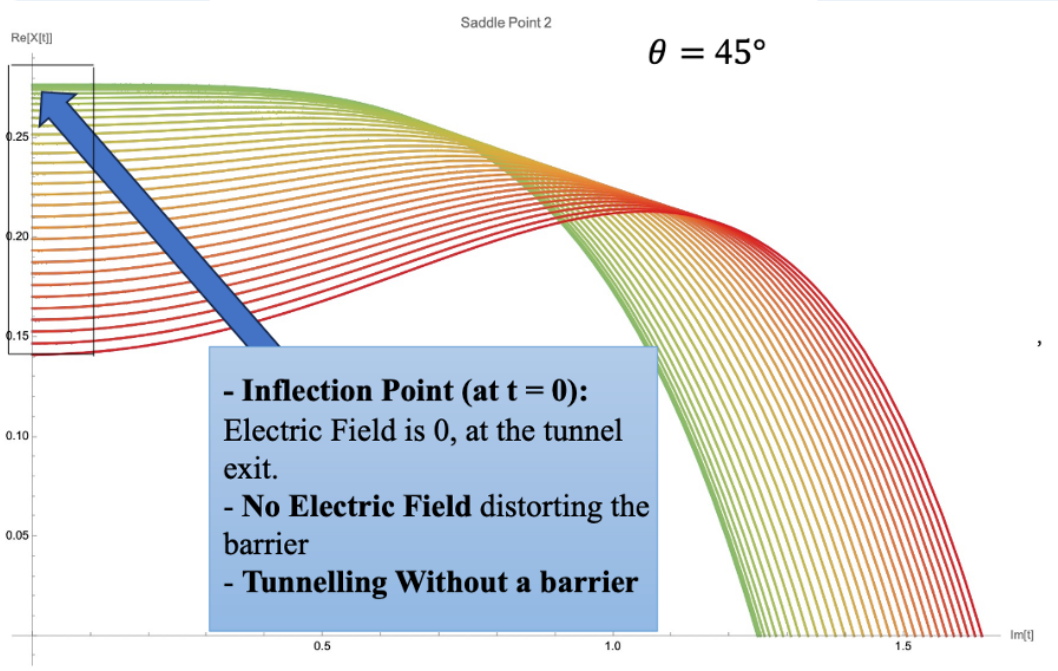


Figure 8: Real Component of the Electron’s Trajectory vs Imaginary Time (time taken for electron to tunnel), for Saddle Point 2 = B (See Figure [6])

Where the same rainbow colour scheme was upheld from Figure [6] (strong positive is red, and strong negative is violet). It seems that there are only contributions from positive to neutral valued momenta, however this plot only represents the real part of the trajectory inside the barrier, the 3D plot of the whole trajectory (real and imaginary) gives a symmetrical shape in momenta which can be viewed in this link here: <https://yannjanssen001.github.io/tunnelingtrajectories/>.

Due to the way the action’s temporal integral is evaluated, and because of the complex nature of the problem, time effectively flows from right to left illustrated in Figure [7]. In Figure [8] there is an inflection point meaning the electric field is zero at the tunnel exit, so there is distortion of the barrier, further demonstrates that tunnelling without a barrier is possible.

It is evident that the electron’s trajectory is governed by the laser’s electric field. While the electron is tunnelling its path is continuously influenced by the oscillations of the driving laser. At the moment of exit (at $t = 0$), there is an inflection point, indicating that there is no electric field present distorting the barrier, meaning tunnelling without a barrier.

Moreover, this is not the only abnormal event that has been observed in the electron’s trajectories. For lower values of mixing angle, $\theta = 15^\circ$, the particle tunnels the wrong way out as shown below.

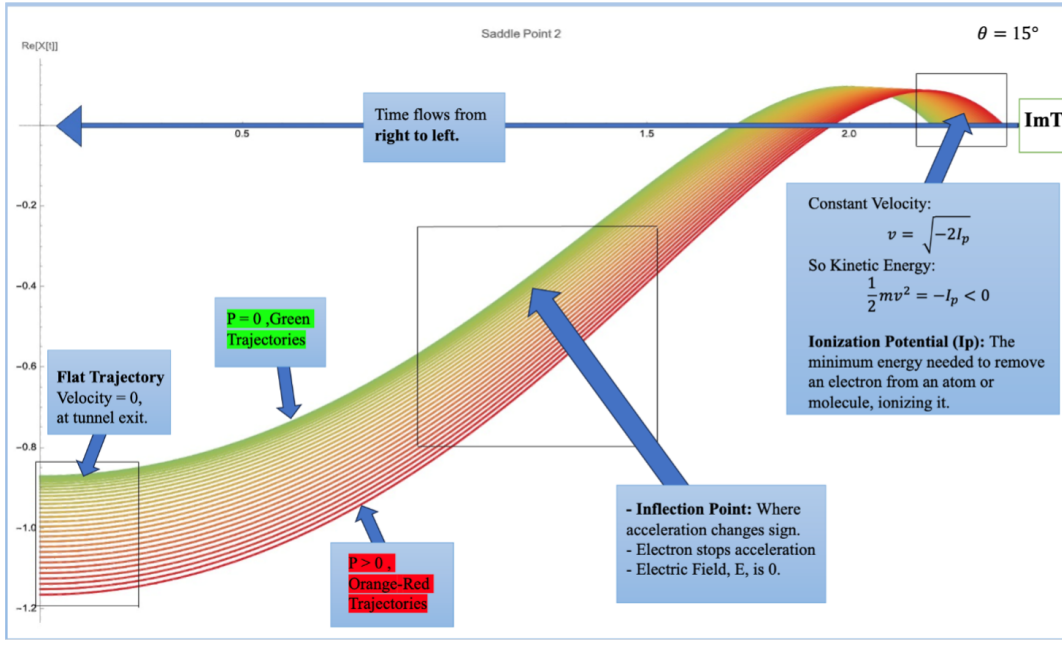


Figure 9: Real Component of the Electron's Trajectory inside the Barrier (Imaginary Time), for Saddle Point 2 = B (See Figure [6])

Just as Figure [8], the momenta's colour scheme is the same, and the trajectory remains symmetric in 3D ([View Here](#)). For this configuration of the mixing angle, the particle tunnels the 'wrong way' and then stops, changes direction, and comes out the other side which becomes clear to view in Figure [10].

If the reader were to rotate this plot [Figure 9] anticlockwise, it would be clear to see the electron follows the abnormal tunnel path drawn in the diagram below [Figure 10].

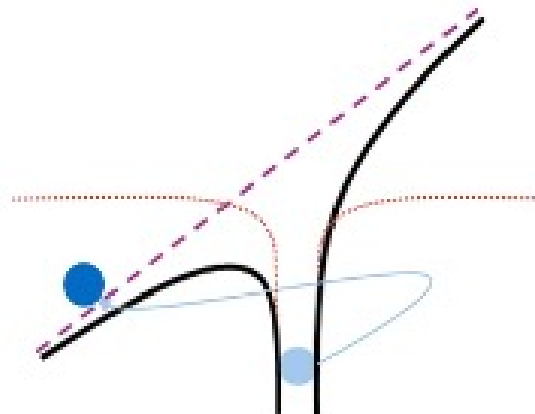


Figure 10: Abnormal Tunnelling Event, Electron Tunnelling the Wrong Way, for Saddle Point 2 = B (See Figure [6])

Furthermore, there is even a case where the electron tunnels out the middle of the potential well for Mixing angle $\theta = 35^\circ$, this is demonstrated in Figure [11] below.

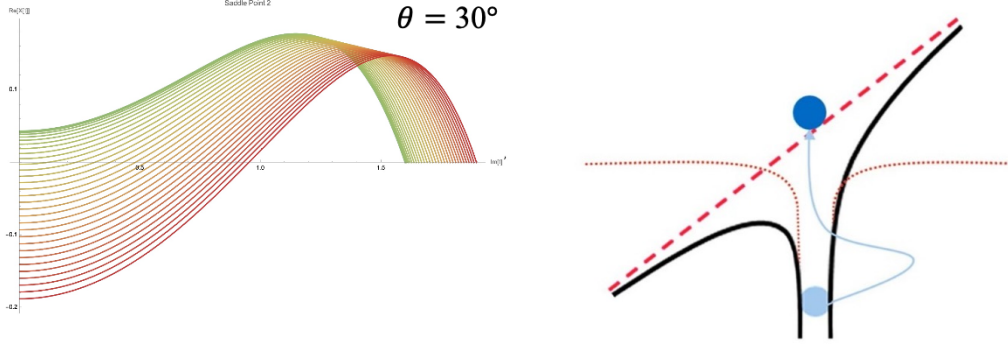


Figure 11: Real Component of the Electron’s Trajectory vs Imaginary Time. Second Abnormal Tunnelling Event: Tunnels the wrong way and exits in the middle of the barrier. For Saddle Point 2 = B (See Figure [6])

Once again this trajectory is symmetrical in momenta, if viewing the whole trajectory, in 3D, real and imaginary components, as previously done in Figures [8][9][10](View Here). These trajectories defy our understanding of quantum tunnelling, creating new opportunities to study the electron’s dynamics in theory, and one day, experimentally. It has been demonstrated how interesting Saddle Point B behaves in Figure [6], throughout the colour switchover, not only at the halfway point $\theta = 45^\circ$ [Figure [8]], but also for lower mixing angles, $\theta = 35^\circ$ [Figure [9]] and $\theta = 15^\circ$ [Figure [11]]. Subsequently, this report will investigate how these saddle points behave for lower values of mixing angles.

2.3 Decreasing Mixing Angles - Coalescence

As the mixing angle decreases from $\theta = 45^\circ$, the electric field will start to transition from bichromatic to monochromatic, meaning that it will go from having two maximas and two minimas to having one maxima and one minima. Since saddle point solutions correspond to the stationary points of the action, which is strongly influenced by the electric field, their behaviour during the transition reveals interesting features worth examining. This transition is captured in the plots below.

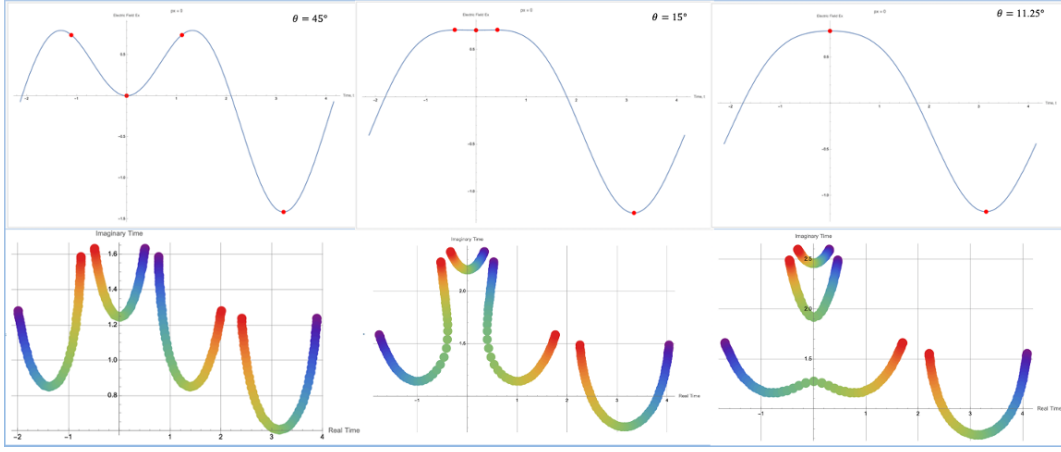


Figure 12: Electric Field vs Time (Top Charts), and its Saddle Points in the Complex Plane (Bottom Chart: Horizontal Axis: Real Time and Vertical Axis: Imaginary Time) for Decreasing Mixing Angles θ .

The saddle points move with the oscillations of the electric field during the colour switchover, near the maxima and minima of the laser field. It is evident that these saddle points merge onto one another, they coalesce on top of one another, at $\theta = 11.25^\circ$, making it seem like there are only two saddle points present, but the saddle point plots in the complex plane shows that there are three shapes laying on top of one another. Where it was Saddle A and C [Figure 6] that merged together, and as the mixing angle decreases, saddle B's contribution decreases significantly as it goes away in an imaginary component of time. When the two saddle points, A and C, merge and momentarily coincide (coalesce), is known as a fold point, creating a degenerate critical point [4].

In Figure [12], it seems as if the saddle points merging together is permanent, however, when bringing the mixing angle even lower to $\theta = 5^\circ$, it becomes clear that it is indeed momentarily.

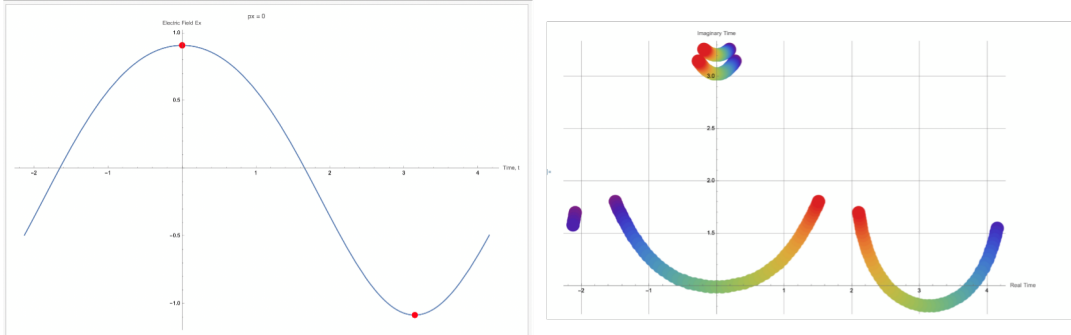


Figure 13: Electric Field vs Time (Top Charts), and its Saddle Points in the Complex Plane (Bottom Chart: Real Time vs Imaginary Time) for Mixing Angle $\theta = 5^\circ$.

It is apparent that saddle points A and C momentarily coincide and merge, and then they eventually split off. It is hard to see which saddle point stays behind and which one goes away into imaginary time along with saddle point B. Under further inspection, one can observe that one half of saddle A and C went away together into complex time, and the other half stayed next to Saddle D.

Moreover, it can be concluded that the significance of saddle point B is extremely low in comparison to that of saddle D, as in Figure [12] there was an instance where Saddle A, B and C amounted to

the same value of Saddle D ($\theta = 11.25^\circ$). This is rather unfortunate, as quantum tunnelling without a barrier was observed for saddle point B. This report will now seek to investigate methods on how to amplify saddle point B's contribution to the action. Therefore, one can ask what happens to the saddle points when another dimension is added to the electric field, the next section will discuss the collinear case, and then the section afterwards, the co-orthogonal case.

3 Saddle Points in a Collinear Electric Field

When adding another dimension to the Electric Field, E_x and E_y , it introduces momentum and electrodynamical vector potential in x and in y too, so the action will change to

$$S(\mathbf{p}, t) = \int_{-\infty}^t \left[I_p + \frac{1}{2} ((p_x + A_x(t'))^2 + (p_y + A_y(t'))^2) \right] dt' \quad (15)$$

and expanding out the brackets gives

$$S(\mathbf{p}, t) = \int_{-\infty}^t \left[I_p + \frac{1}{2} (p_x^2 + 2p_x A_x(t') + A_x^2(t') + p_y^2 + 2p_y A_y(t') + A_y^2(t')) \right] dt' \quad (16)$$

where one can say that the collinear case produces a one dimensional electric field [1.3.2]. As one component of the electric field, E_x , will have the two colour laser (13) and the orthogonal component, E_y , will be zero. Therefore, the EM vector potential in the y direction, A_y , will also be zero. The action for 2D Electric Field for the Collinear case (E_x and $E_y = 0$) gives

$$S(\mathbf{p}, t) = \int_{-\infty}^t \left[I_p + \frac{1}{2} (p_x^2 + 2p_x A_x(t') + A_x^2(t') + p_y^2) \right] dt' \quad (17)$$

where p_y^2 can be treated as constant, and can be absorbed into the ionisation potential, creating an effective ionisation potential, leaving the action to be the same as Quantum Tunnelling Without a Barrier Section [2],

$$S(\mathbf{p}, t) = \int_{-\infty}^t \left[I_p^{\text{eff}} + \frac{1}{2} (\mathbf{p} + \mathbf{A}(t'))^2 \right] dt' \quad (18)$$

which will then be just magnified case from Weber's paper on Quantum Tunnelling Without a Barrier[15]. Additionally, it can be expected that the collinear case will be symmetrical to the one in Quantum Tunnelling Without a Barrier Section [2] and Weber's paper [15]. This can be illustrated after having found the saddle point solutions (2) to the collinear action equation (18), and is demonstrated in the plots below.

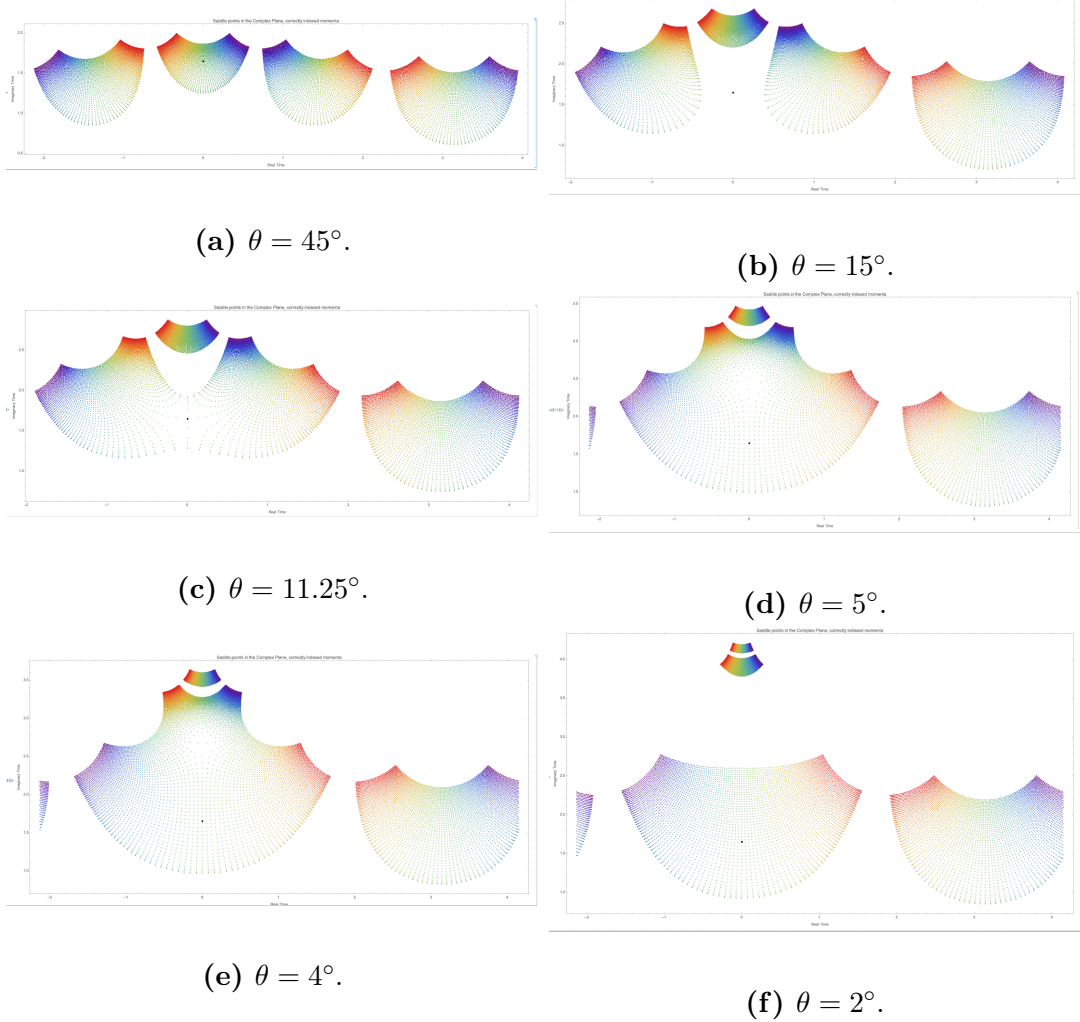


Figure 14: Saddle points in the Complex Plane (Horizontal Axis: Real Time and Vertical axis: Imaginary Time) for different mixing angles (See Formula (13))

These are the saddle points solutions during the colour switchover, starting from the halfway point and lowering the mixing angles to reach the monochromatic case (where $\theta = 0^\circ$). These Saddle points are plotted in the Complex Time plane, where the y axis is Imaginary time, and the x axis is real time, and the same rainbow colour scheme used throughout this paper is implemented for momentum in the x direction (p_x). It is evident that these are as identically symmetrical as those in Figures [12] and [13], however in the collinear case, there are multiple combinations of p_x and p_y , creating multiple lines of saddle point solutions as seen in Figures [12] and [13], creating this symmetrical thimble looking shape.

It is apparent that Saddle A and C move closer to one another when decreasing the mixing angle, and eventually they momentarily coalesce creating a fold point in Figure [14c]. As the mixing angle keeps decreasing, the saddle points separate in the following way: half of saddle A and half of saddle c combine and go away in imaginary time, whilst the other half of A and C merge and amplify in presence as they stay and become the saddle point for the monochromatic electric field. These are identical trends seen with the saddle point solutions in the Quantum Tunnelling Without a Barrier Section 2.

3.1 3D View Saddle Points [p_y , Real time, Imaginary Time]: Channel Structures at Coalescence

A fold point is when two saddle points merge and coincide momentarily, creating a degenerate critical point [4], which is apparent in Figure [14c]. To view this in more detail the momentum in y direction is added to Figure [14c] above, and Figure [15] below, where various angles of the resulting 3D plot are shown.

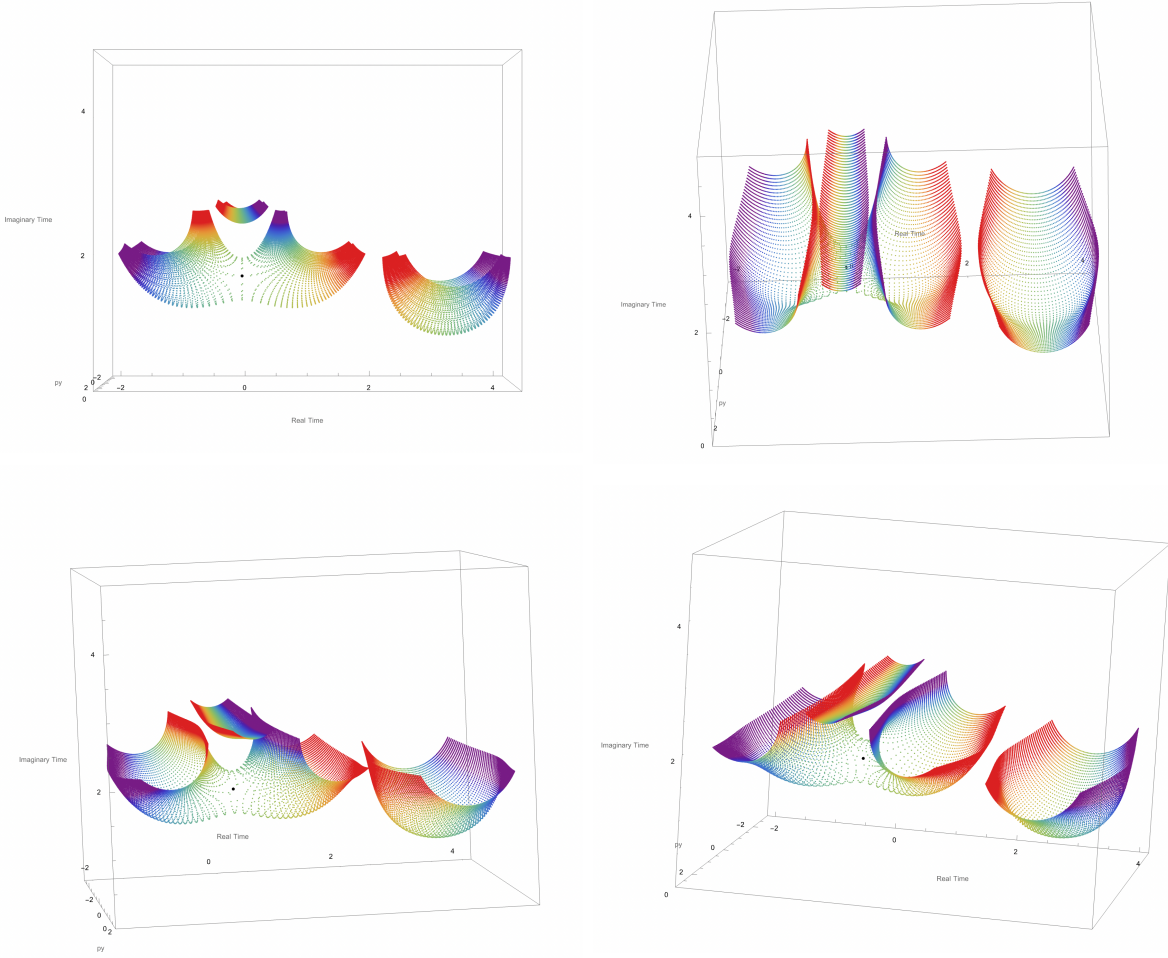


Figure 15: Top left is the same as Figure [14] but in 3D. The other 3D plots show the saddle points as a function of time (Real time is horizontal, imaginary time is vertical) and momentum p_y (into the page). So this is a four dimensional object since momentum p_x is colour coded in these plots with the same rainbow scheme

The coalescence of these saddle points create a channel between the two saddles (A and C) and the degenerate critical point lays in the centre of it (fold point). To view the colour switchover occur in 3D, and get a better view of this channel, refer to this link [here](#).

The fold point is the centre of this symmetrical aesthetically pleasing object, allowing a clean connection between saddle A and C. This is because the complex valued ionisation times and momenta in x and y are known for all saddle points, including the fold point, which makes up this

shape.

It has been made obvious that saddle D is significantly stronger than saddle A, B and C. The saddles A, B, and C amplitude contributions to the integral contour are mixed up due to the coalescence observed in Figure [15] [12]. In the prior section 2, saddle point B's solutions and electron trajectories whilst tunnelling has shown interesting and un-intuitive behavior. This report wants to make saddle B's contribution to the integral contour more significant, but unfortunately the collinear electric field only amplified the saddles in section 2, making those two symmetrical to one another.

Furthermore, measuring which saddle contributes to the integral contour is difficult due to the coalescence [12][15]. During the colour switchover, it is hard to keep track of which saddle is which during coalescence, as two saddle points merge momentarily and then split off, one going into high values of complex time and other staying put, as observed in Figure [14]. Classification of these saddle point has been done, as there is one fold point during coalescence that can be used to track which half of A merges with C, making this saddle structure completely distinguishable [15]. However, this does not help amplify saddle B's presence into the integral contour, as saddle A and C coalesce ontop of saddle B, and saddle D's overwhelming presence removes any sort of significant and measurable contribution from saddle B [12].

Perhaps a co-orthogonal electric field will alter the saddle points structure to significantly amplify saddle B's amplitude contribution to the integral contour, and to have classified a distinguishable saddle point structure would been a bonus. This could allow measurement of individual saddles, which would amplify the significance of saddle point B to further investigate how these un-intuitive electron trajectories behave, and even proceed to calculate its quantum orbital yields (quantifying its significance) [12].

4 2D Extension: Co-Orthogonal Field

For the co-orthogonal case, the action with 2D electric field (15), will be with the first harmonic in one direction [$E_x = E_1 \cos(wt)$] (13) and the second harmonic [$E_y = E_2 \cos(2wt)$] (13) perpendicular to that direction, to produce a co-orthogonal electric field as shown in Figure 5.

Finding the saddle point solutions for the co-orthogonal action will produce the following plots during the colour switchover:

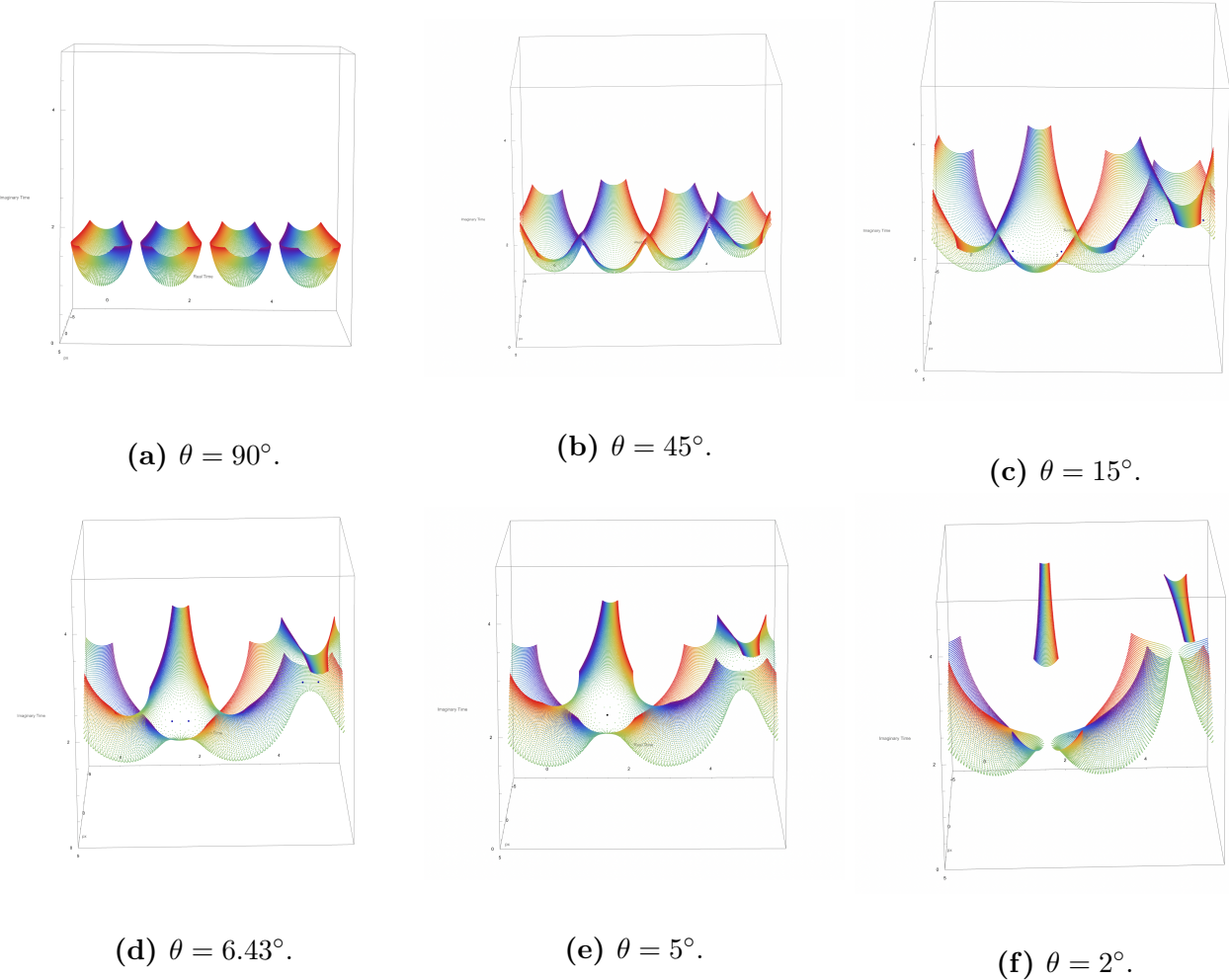


Figure 16: Co-orthogonal Electric Field: 3D plots show the saddle points as a function of time (Real time is horizontal, imaginary time is vertical) and momentum p_x (into the page). So this is a four dimensional object since momentum p_y is colour coded in these plots with the same rainbow scheme

The saddle points form a canoe-like structure, which can be better viewed as a 3D GIF here <https://yannjanssen001.github.io/SaddlePointsFor2DElectricField/>. The changes of this saddle point structure are different from the prior cases in section 2 and 3, as these saddle point objects are touching one another (At $\theta = 45^\circ$). The saddle point structure is demonstrating a sort of path connectivity, in terms of their amplitude contributions to the Feynman path integral [12]. It is apparent that the saddle point structure is self-intersecting at nature. When decreasing the

mixing angle θ , these canoe-like structures start to come closer together, making it self intertwine further. Due to this self entanglement of the saddle point structure, it becomes hard to distinguish which saddle is which, as before, for the 1-dimensional case [2 and 3], the structure was already classified with a rigid structure. Hence, a classification problem is presented for the co-orthogonal case.

Before tackling this classification problem, there is something very fascinating occurring with the saddle point structure in Figure [16]. On the topic of path connectivity, these saddle points are self intersecting at a fold point. In the previous section, the saddle point structure coalesced into one fold point, however, in Figure [16], the saddle point structure contains three fold points separating the four canoes within one periodic cycle of the laser oscillation (time). Additionally, for lower values of mixing angle θ , the canoe objects come closer together and eventually coalesce, meaning that there are two fold points momentarily merging together and coinciding into one cusp point. Essentially, there are two merged saddle points coinciding with another two merged saddle points coalescing into four merged saddle points. Before moving any further, let's dive into Bifurcation Theory.

4.1 Bifurcation Theory

Bifurcation theory is the study of a sudden change in the qualitative behavior of a dynamical system when varying a parameter [9][6]. The saddle point solutions that satisfy the action (15), coalesce and self intersect when varying the mixing angle θ as shown in Figure [16], hinting a deeper connection to bifurcation theory. Understanding these saddle point transitions, referred to as bifurcations, is essential to determine what these folds and cusps mean. They can be interpreted as a new solution emerging, the disappearance of solutions, or the merging of multiple states into a single one [9][6].

The saddle points represent a critical point in the action for this quantum system, and as shown in Figure [16], the transition from distinct saddle points to self-intersecting and intertwined structures reflects a bifurcation in the system [9][6].

Initially, the saddle point structures are distinct, then, as the mixing angle decreases, they begin to merge. In Figure [16], the coalescence of these saddle points is what is causing this self intersecting structure [9][6]. The study of the fold bifurcation, when two solutions collapse into one, can help understand this saddle point structure [9][6].

A fold bifurcation leads to significant qualitative changes for the system [9][6]. These saddle point solutions are ionisation times which initially exist at separate moments for given electron's drift momentum (rainbow colour scheme in Figure [16]). As the mixing angle decreases, the two ionisation times approach one another, and eventually merge into a single ionisation time, marking a critical transition in the system's behaviour [9][6].

Evaluating the colour switchover even further, for lower values of the mixing angle θ , these fold points approach one another and eventually merge into a single cusp point. Essentially, what was originally four ionisation times, coalesced into two collapsed ionisation times, which coalesced once more into one double collapsed ionisation times. This marks a higher order bifurcation, where two

prior distinct fold bifurcations merge to form a cusp bifurcation [9][6]. The physical meaning of this transition results in a more intricate and entangled structure, as two sets of merged saddle points coalesce causing a significant shift in the system's dynamics [9][6].

Understanding bifurcations is crucial as they provide insight into how quantum systems can change under small variations in parameter, suggesting direct implications for the understanding its quantum dynamics [9][6]. This can be used as a powerful tool for predicting and controlling the behavior of complex systems, and guide future experiments such as quantum control and quantum state manipulation [9][6].

As these saddle points coalesce (Figure [16]), either through fold bifurcations or cusp bifurcations, the system becomes more of a self-entangled structured. This process of merging saddle points, and the associated topological changes, will be crucial for solving the classification problem posed by the intertwining saddle points and gaining a deeper understanding of the system's path connectivity.

4.2 Identifying and Tracking Fold and Cusp Points

The condition to identify the fold bifurcation in Figure [16], is for the fold points to satisfy these equations below [4].

$$\frac{\partial S(\vec{p}, t_s)}{\partial t} = 0, \quad \frac{\partial^2 S(\vec{p}, t_s)}{\partial t^2} = 0, \quad (19)$$

and for the cusp bifurcation [4],

$$\frac{\partial S(\vec{p}, t_s)}{\partial t} = 0, \quad \frac{\partial^2 S(\vec{p}, t_s)}{\partial t^2} = 0, \quad \frac{\partial^3 S(\vec{p}, t_s)}{\partial t^3} = 0 \quad (20)$$

where momentum is now a vector in x and y since the electric field is 2-dimensional, different to the 1D case (2). So for the fold bifurcation there are four equations (2-dimensional momentum and action) and four unknowns since ionisation time t_s is complex (19). The cusps bifurcation, there are six equations and six unknowns, if mixing angle is treated initially as complex just for the sake of matching the dimensionality of equations to solve and variables to find. This can be solved numerically through simultaneous equations, and in the case of the cusps, the solutions were filtered to only accept real valued mixing angles as its more of a physical solution to deal with.

The real and imaginary components of the ionisation times, momentum in x and y for the fold and cusps points are known for real valued mixing angles. The fold points were plotted in momentum space over the colour switchover to see how they evolve. A rainbow colour scheme was used here to indicate initial values of the mixing angle θ as violet and final values as red.

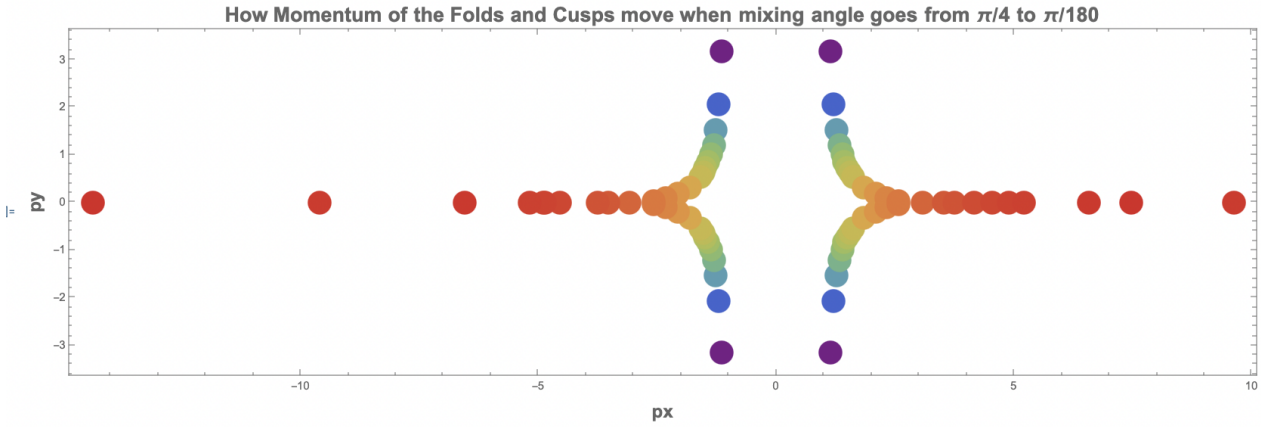


Figure 17: How the fold points (19) from Figure [16] evolve throughout the colour switchover in momentum space (p_x, p_y) , clearly displaying bifurcation set of cusp catastrophe [4]. The rainbow colour scheme here was used differently, to display the beginning of the colour switchover, bichromatic case (Violet), transitioning to the monochromatic case (Red).

It is evident that the evolution of this system contains two cusp bifurcations. The bifurcation set of a cusp catastrophe is when two solutions collapse into one, and in Figure [17] it shows that there are two cusps present in this saddle point structure (Figure [16]) [4].

These fold and cusp bifurcations are the reasons behind the self intersecting structure seen in Figure [16]. They are vital in the classification problem posed with the self-intertwining nature of the saddle points structure.

4.3 Nine-Fold Classification through Fold Bifurcation

The saddle point structure is highly self intersecting due to the folds present in Figure [16]. Since the definition of fold is two solutions collapsing into one, there will be multiple saddle point solutions with the same values, making its manifold structure self intertwine. Through that reasoning, it could be possible to untangle this self intertwined structure using these fold bifurcations.

The momentum of the fold points are known as shown in Figure [17], and there are four fold points. One can create nine regions in momentum space based on the four fold points as shown below in Figure [18].

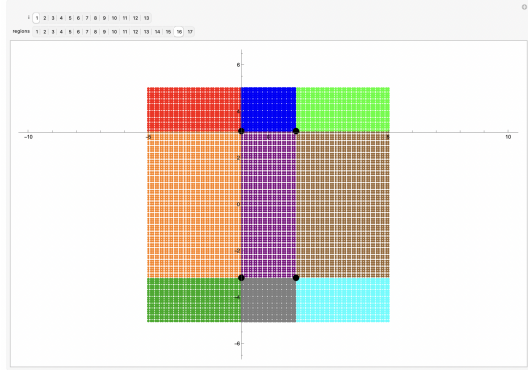


Figure 18: The violet dots (Fold points) from Figure [17] are the black dots plotted here, creating regions in momentum space (p_x, p_y) labelled through colours. This is one mixing angle configuration $\theta = 45^\circ$, this is done for all the fold points in the bifurcation set of a cusp catastrophe (Figure [17])

Making each region follow certain conditions, such as greater than or less than one of the fold's momentums. These saddle points can be sectioned into the same corresponding regions in momentum space. This is shown in the figure below where the saddle point structure was sectioned in momentum space and plotted in p_x , real time and imaginary just as the original saddle point structure (Figure [16], for 3D GIF of the colour switchover effect on these dissected saddles can be seen at the bottom of this linked page).

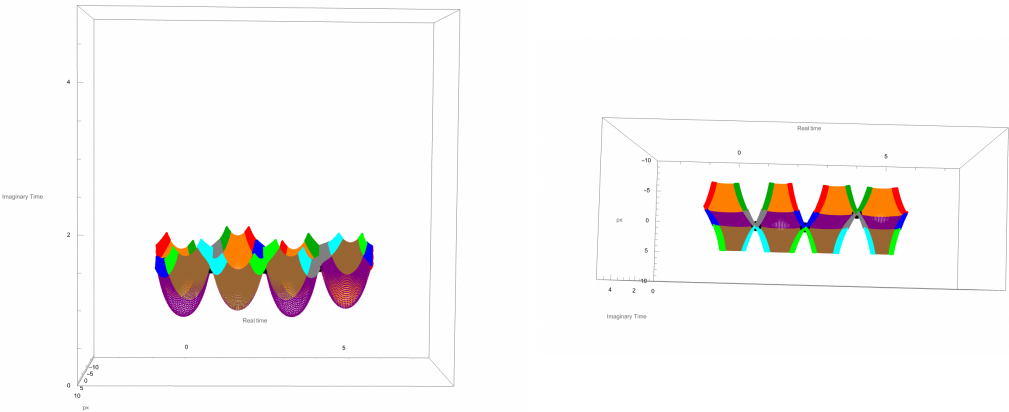


Figure 19: Co-orthogonal Saddle Point Solution Structure [(Real time is horizontal, imaginary time is vertical) and momentum p_x (into the page)] from Figure [16], sectioned based off the momentum space regions displayed in Figure [18].

Every momentum combination generates four saddle point solutions as seen in Figure [6], so each region will have four trajectories. Matching the colours from the momenta space regions created in Figure [18] to Figure [19], it becomes evident that there are four distinct orbitals per momentum region. In addition, the self-intersecting nature seen in Figure [16] is no longer present for this configuration of mixing angle here ($\theta = 45^\circ$). One can dissect these saddle points into four distinct objects. One needs to cut the fold points by their corresponding real time values to successfully perform surgery and dissect this structure into four distinguishable objects. This is shown in the

figure below, where classification for the saddle point structure was a success for mixing angle values for fold bifurcation.

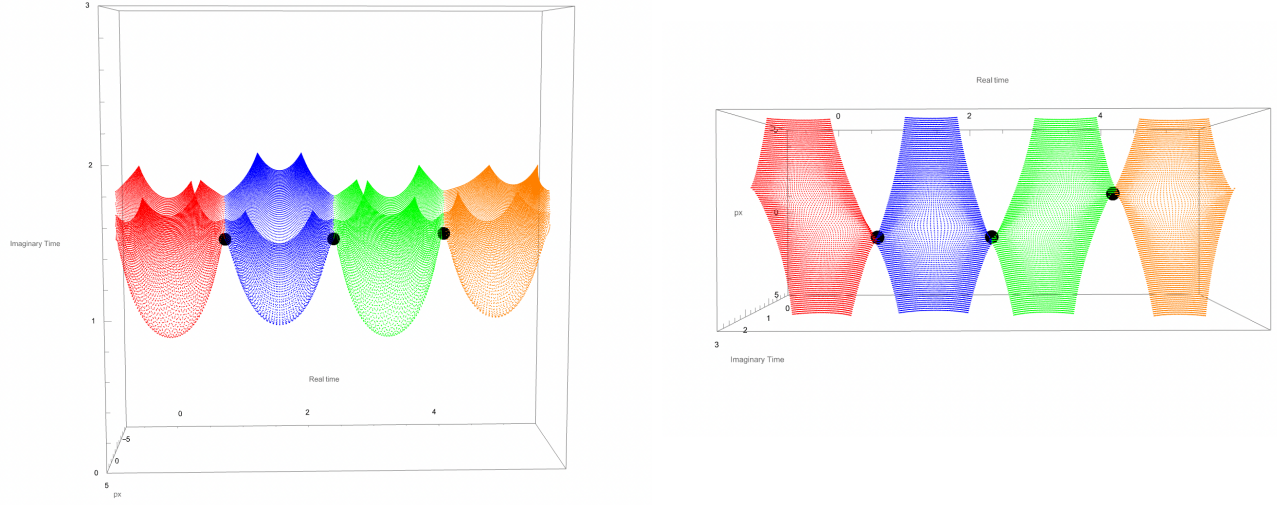


Figure 20: Post-Surgery Saddle Point Structure [(Real time is horizontal, imaginary time is vertical) and momentum px (into the page)], clearly classified, labelled as Red, Blue, Green, and Orange.

Now, this structure is classified as Red, Blue, Green and Orange (RBGO), but bare in mind that they do not correspond to the same quantum orbitals A,B,C and D as observed in the 1-dimensional case (Figure [6], [for 3D GIF of the colour switchover effect on these dissected saddles can be seen at the bottom of this linked page](#)). This is the correct approach on how to classify coalescing self intersecting saddle points. This will be done for all fold points present in Figure [17], when the two folds collapse into a cusp, there will be six momentum regions instead of nine. This is further explained in the next sub-section, as the same procedure is used to classify the saddle point structure in the cusp regime (for lower mixing angle values).

4.4 Six-Fold Classification through Cusp Bifurcation

The same technique for nine-fold classification through fold bifurcation is done now for the cusp bifurcation. This becomes a six-fold classification due to the six regions created in momentum space by the two cusp points.

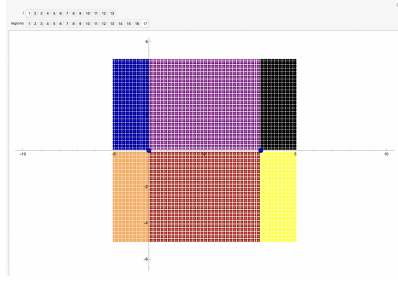


Figure 21: Cusp points from Figure [17] creating regions in momentum space (p_x, p_y) labelled through colours

The lower values of the mixing angles where cusp bifurcation occur due to the coalescence, it seems that there are now three quantum orbitals separated by the two cusp points. Thus, there will be three trajectories for every one of the six regions in momentum space. The surgical dissection of these saddle points in momentum space is done again as was done in 4.3.

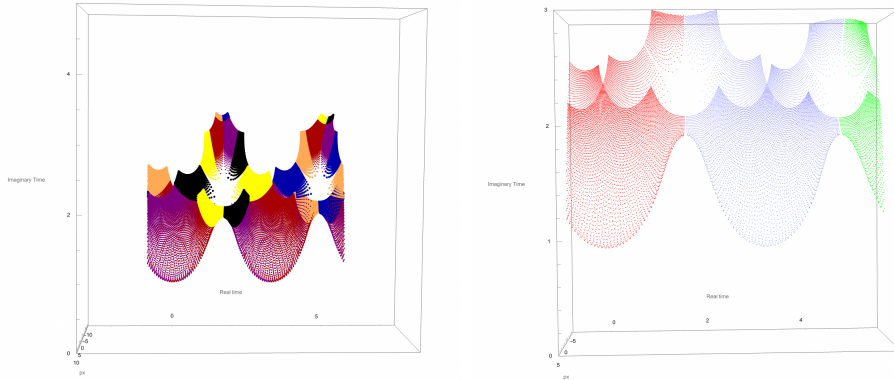


Figure 22: Left Figure: Co-orthogonal Saddle Point Solution Structure [(Real time is horizontal, imaginary time is vertical) and momentum p_x (into the page)] from Figure [16], sectioned based off the momentum space regions displayed in Figure [21]. Right Figure: Post-Surgery Saddle Point Structure [same axis], labelled as Red, Blue and Green.

where the Red, Blue and green orbitals are different to the RBGO orbitals done for the fold bifurcation in subsection 4.3, [for 3D GIF of the colour switchover effect on these dissected saddles can be seen at the bottom of this linkedpage]. At first glance it may seem that this was another successful surgery once having cut through the cusp's real time values. However, an aerial view of this plot is shown below, where self intersecting nature is still present.

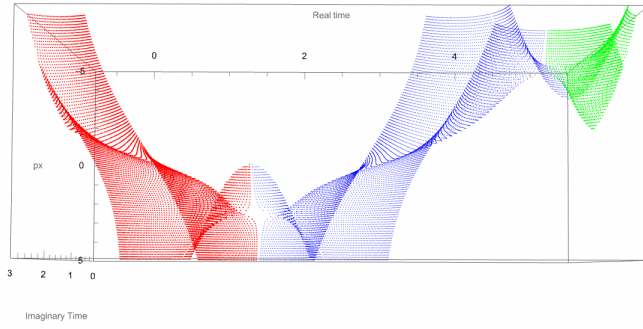


Figure 23: Aerial View: The right 3D plot in Figure [23]. Post-Surgey Saddle Point Structure [(Real time is horizontal, imaginary time is vertical) and momentum px (into the page)], labelled as Red, Blue and Green. Self Intersecting Nature is Present!

At low mixing angle, this saddle point structure for the cusp bifurcation is still highly self intersecting. Further analysis of how these saddle points behave in the cusp bifurcation regime is needed. One needs to plot the momentum space against the real component of time [px, py, Ret] and separately examine into its imaginary counterpart of time [px, py, Imt]. Remember, this is a six dimensional problem as discussed in previously [4.2], meaning it has a really complicated looking structure. This will allow for further inspection on how the topology of these saddle points behave within the cusp bifurcation regime (highly self intersecting area). It can be said that dissecting the saddle point structure based on the real time of the cusps would have not fully separated them into distinct quantum orbitals. However, cutting the cusp based on its corresponding imaginary component of time could solve this issue and dissect this structure into distinguishable non-self intersecting objects. As the cusps occur at similar, if not identical, real component of time, whilst its complex counterpart varies. This indicates that the object may be self intertwining, as the real component of time has repeating identical values for cusps during the colour switchover.

Furthermore, being able to classify these saddle points will allow surface plotting (parametric plots) instead of individually plotting every saddle point solution. This is less computationally taxing in comparison to creating a shape using dots (saddle points). In addition, and most importantly, it will allow better interpretation of the shape of this saddle point structure as its easier to see past the self intertwining nature of these saddle points in surface plots (parametric plots).

This paper has successfully been able to classify the saddle points for the co-orthogonal electric field case for majority of the colour switchover, from Bichromatic configuration $\theta = 90^\circ$ for the fold points until the beginning of the cusp bifurcation regime. Once these fold points coalesce and merge, further study of the cusp bifurcation regime is needed to fully classify the saddle point structure for smaller values of θ .

5 Conclusion

Quantum tunnelling remains a cornerstone of attosecond science, enabling the exploration of ultrafast electron dynamics. In this study, we investigated a surprising ionisation event which occurs in the absence of the coloumb potential barrier (when the electric field is zero), challenging conventional models of strong-field induced tunnelling. Due to its extremely low yield, detecting this process experimentally is difficult, motivating a deeper theoretical understanding. To address this, we employed a topological saddle point analysis combined with bifurcation theory, extending the electric field into two dimensions and exploring collinear and co-orthogonal configurations. For the collinear case, an amplified version of the 1-dimensional case explored in Weber's paper [15], and section 2. This provided a greater understanding of the symmetry around the fold point generated in the channel structure [15], path discontinuity between saddle points, and aesthetically pleasing shape. Contrastingly, the co-orthogonal case revealed a rich, self-intersecting saddle point structure that evolves with the mixing angle of the two-colour field, a process we refer to as the colour switchover. As this angle varies from bichromatic to monochromatic configurations, we observe fold and cusp bifurcations that complicate the classification of quantum trajectories. As these bifurcations were the case of the highly self intersecting objects, since it leads to the collapse of multiple solutions to fewer solutions. This overlap may be the cause of our problems but also led us to our solutions. By applying bifurcation theory, we propose a systematic methodology for analysing these complex structures. Whilst this approach does not directly enhance the yield of the barrier-free ionisation event, it provides valuable insights into the underlying topology of the process and may suggest new directions for identifying experimentally accessible signatures.

References

- [1] Anne L’Huillier. Nobel Prize lecture: Anne L’Huillier, Nobel Prize in Physics 2023. <https://www.youtube.com/watch?v=QFYyduL9WZA>, 2023. Nobel Prize, Accessed: 2025-04-14.
- [2] Luke Edward Chipperfield. *High Harmonic Generation with Few-Cycle Pulses*. PhD thesis, Quantum Optics and Laser Science Group, The Blackett Laboratory, Imperial College London, London, United Kingdom, 2005.
- [3] N. B. Delone and V. P. Krainov. Tunneling and barrier-suppression ionization of atoms and ions in a laser radiation field. *Physical Review Letters*, 71(13):1994–1997, 1993.
- [4] F. W. J. Olver et al. *NIST Digital Library of Mathematical Functions*. National Institute of Standards and Technology, 2023. Release 1.1.11 of 2023-09-15.
- [5] David J. Griffiths. *Introduction to Electrodynamics*. Pearson Education UK, 4 edition, 2013.
- [6] John Guckenheimer. Saddle-node bifurcation. In Werner Dubitzky, Olaf Wolkenhauer, Kwang-Hyun Cho, and Hiroki Yokota, editors, *Encyclopedia of Systems Biology*, pages 1891–1892. Springer, 2013.
- [7] Eugene Hecht. *Optics*. Addison-Wesley, Reading, Massachusetts, 4th edition, 2002.
- [8] Christian Kern, Michael Zürch, and Christian Spielmann. Limitations of extreme nonlinear ultrafast nanophotonics. *Beilstein Journal of Nanotechnology*, 7:1176–1183, 2016. Open Access Review Article, Accessed: 2025-04-14.
- [9] Caitlin McCann. Bifurcation analysis of non-linear differential equations, May 2013. Supervisor: Dr. Vasiev.
- [10] Edmund Optics. Introduction to polarization. <https://www.edmundoptics.com/knowledge-center/application-notes/optics/introduction-to-polarization/>. Accessed: 2025-04-15.
- [11] S. V. Popruzhenko. Keldysh theory of strong field ionization: history, applications, difficulties and perspectives. *Journal of Physics B: Atomic, Molecular and Optical Physics*, 47(20):204001, 2014.
- [12] P Salières, B Carré, L Le Déroff, F Grasbon, GG Paulus, H Walther, R Kopold, W Becker, DB Milošević, A Sanpera, and M Lewenstein. Feynman’s path-integral approach for intense-laser–atom interactions. *Science*, 292(5518):902–905, 2001.
- [13] Thomas Schultz and Marc Vrakking. *Attosecond and XUV Physics: Ultrafast Dynamics and Spectroscopy*. Wiley-VCH, Weinheim, 2014. Accessed: 2025-04-14.
- [14] Olga Smirnova and Misha Ivanov. Multielectron high harmonic generation: Simple man on a complex plane. *arXiv preprint arXiv:1304.2413*, 2013.
- [15] Anne Weber, Margarita Khokhlova, and Emilio Pisanty. Quantum tunneling without a barrier. *Physical Review A*, 111(4):043103, 2025.

- [16] Wikipedia contributors. Saddle point — Wikipedia, the free encyclopedia, 2024. Accessed: 2025-04-15.